Impact of Topographic Normalization on Land-Cover Classification Accuracy

Stephen R. Hale and Barrett N. Rock

Abstract

For pixel classifying algorithms to perform effectively, effects of topographic relief must be minimized or removed. In areas of high topographic relief, problems arise when spectral variations in ground target illumination and radiance, owing to differences in incident radiation and non-Lambertian reflectance behavior, respectively, cause identical land-cover types to reflect differently, or different cover types to reflect similarly. A Landsat Enhanced Thematic Mapper image was processed using band ratios, the Minnaert Correction, aspect partitioning, and combinations of these treatments to generate independent land-cover classifications. Treatment classification accuracy was determined using error matrices and the Kappa statistic. Producer's and User's Accuracies were examined to determine if treatments were superior at producing greater class-specific accuracy. None of the treatments produced a significantly more accurate classification; however, assessment of class-specific accuracies indicated accuracy gains using aspect partitioning alone or in combination with the Minnaert Correction.

Introduction

Remote sensing of montane landscapes, characterized by high topographic relief, presents challenges to land-cover classification not encountered on level or constant terrain. Several authors noted reduced accuracy in classifications of mountainous regions (Teillet *et al.*, 1982; Colby, 1991; Ekstrand, 1996). Problems arise when spatial variations in ground target illumination and radiance, owing to differences in incident radiation and non-Lambertian reflectance behavior, cause identical surface features (e.g., land-cover types) to reflect differently, or cause different surface features to reflect similarly. For pixel classifying algorithms to perform effectively, effects due to topographic relief must be minimized or removed.

Several topographic normalization techniques are available for nadir viewing sensors, but few studies have compared their effectiveness in land-cover classification. The Landsat Thematic Mapper (TM) 5/4 band ratio successfully characterized softwoods health in mountainous terrain of New England, (Rock *et al.*, 1986; Vogelmann and Rock, 1988; Vogelmann and Rock, 1989; Vogelmann 1990). Colby (1991) compared variability of brightness values (BVs) from band-ratios and the Minnaert Correction of lodgepole pine (*Pinus contorta*) stands in Colorado, and concluded that both procedures effectively reduced variation in BVs, and the Minnaert Correction more so. The Minnaert Correction, first used to describe the moon's surface roughness (Minnaert, 1941) and adapted for terrestrial remote sensing, accounts for incidence angle and non-Lambertian reflectance properties of montane landscapes. Ekstrand (1996) found that the TM 5/4 ratio, Normalized Difference Vegetation Index (NDVI), and Minnaert Correction performed well at removing the topographic effect in a defoliation study in norway spruce (*Picea abies*) stands in Sweden, but that the TM 5/4 ratio failed to outperform against a single-band near-infrared variable under conditions of moderate defoliation and no chlorosis (Ekstrand, 1994).

The objective of this study was to determine the normalization method or combination of methods, for a nadir-viewing sensor, producing the most accurate classification over a large geographic extent, using general and few cover types. Normalization strategies investigated were (1) aspect partitioning, (2) band ratios, (3) the Minnaert Correction, and (4) combinations of these strategies. Aspect partitioning geographically stratifies an image into subsets with pixel aspect values within or equal to 180 degrees of the solar azimuth ("sunlit" image) and greater than 180 degrees from the solar azimuth ("sunshade" image). Image subsets are classified separately using training sites from within the respective subset, and classifications are subsequently merged back into the full study area. Aspect partitioning is not, in a strict sense, a normalizing method because there is no spectral adjustment of pixel values. However, its inclusion here is based on its potential for classification improvement. The cosine correction method was not treated due to its well documented problem of over-correcting BVs at incidence angles near 90°, causing 8-bit radiometric data to saturate (Teillet *et al.*, 1982; Eckstrand, 1996).

Methods

A cloud-free Landsat Enhanced Thematic Mapper (ETM) scene (Path 13/Row 29; 31 August 1999) was reduced to include areas from 610 m to 1525 m elevation within the White Mountain National Forest, New Hampshire (WMNF; 43°N, 71°W; Plate 1). Absolute georeferencing of image control and validation points improved image rectification to better than 1 pixel (RMSE = 0.97 pixels), and assured plot sampling corresponded with representative training spectra. Diffuse sky irradiance was ignored, and, because this scattering most greatly affects shorter wavelengths, bands 1 and 2 were not used in the analyses. Dark-pixel subtraction was performed on the remaining reflective bands (3 to 5 and 7). More thorough dark-object correction was omitted for lack of targets at the study site elevation and within 80 km.

A digital elevation model (DEM) was assembled from USGS Level 1 DEM quadrangles and was nearest-neighbor resampled to a 28.5-m grid spacing to match the base

Complex Systems Research Center, University of New Hampshire, Durham, NH 03824-3525 (steve.hale@unh.edu; barry.rock@unh.edu).

Photogrammetric Engineering & Remote Sensing
Vol. 69, No. 7, July 2003, pp. 785–791.

0099-1112/03/6907–785$3.00/0

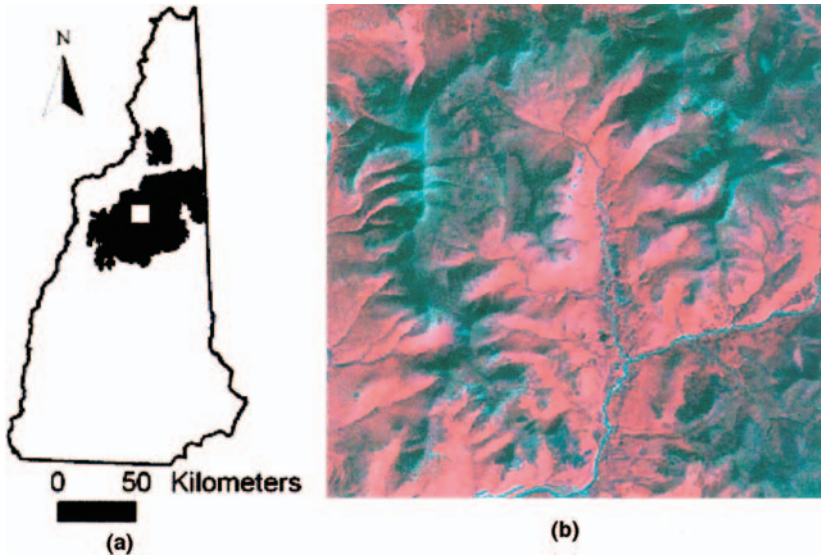

Plate 1. (a) White Mountain National Forest (shaded) within New Hampshire. (b) Composite (4, 3, 2) of inset box (a) showing the topographic effect. Darker and brighter areas occur on northwest and southeast facing slopes, respectively.

image (Civco, 1989). Two iterations of a 3 by 3 low pass filter were applied to remove systematic errors from the final DEM (Brown and Bara, 1994). Slope and aspect images were derived from the DEM image. Derivation of the Minnaert Correction (Smith *et al.*, 1980; Teillet *et al.*, 1982; Colby, 1991) relationship between observed and normalized BVs under the non-Lambertian assumption is given as

$$BV_{o(\lambda)} = BV_{n(\lambda)} \cos^{k(\lambda)} i \cos^{k(\lambda)-1} \theta_n \quad (1)$$

where $k_{(\lambda)}$ is the Minnaert Constant for band λ, $BV_{n(\lambda)}$ is the normalized brightness value of band λ, $BV_{o(\lambda)}$ is the observed brightness value of band λ, θ_n is the surface slope, and i is the incident angle of the solar beam.

The cos i term can be calculated by

$$\cos i = \cos(90 - \theta_s)\cos\theta_n + \sin(90 - \theta_s)\sin\theta_n \cos(\Phi_s - \Phi_n) \quad (2)$$

where θ_s is the solar elevation, Φ_s is the solar azimuth, θ_n is the surface slope, and Φ_n is the surface aspect.

Linearizing Equation 1 using a log transformation yields

$$\log(BV_{o(\lambda)} \cos\theta n) = \log BV_{n(\lambda)} + k_{(\lambda)}(\log\cos i \cos\theta_n). \quad (3)$$

Equation 3 is in the slope-intercept form of a line ($y = b_0 + b_1 x$), and regression of ($BV_o \cos\theta_n$) versus ($\log\cos i \cos\theta_n$) generates the slope estimate b_1, which equals the Minnaert Constant $k_{(\lambda)}$. The empirically derived $k_{(\lambda)}$ is substituted into the Backwards Radiance Correction Transformation (Smith *et al.*, 1980; Colby, 1991), and $BV_{n(\lambda)}$ is found by

$$BV_{n(\lambda)} = (BV_{o(\lambda)} \cos\theta_n)/(\cos^{k(\lambda)} i \cos^{k(\lambda)}\theta_n). \quad (4)$$

The Minnaert Constant is a misnomer, because the slope coefficients are cover-type dependent (Teillet *et al.*, 1982). Estimating cover-type specific Minnaert Constants requires *a priori* knowledge of cover types, but, because land-cover information is sought, these constants are unknown. Vegetated coregistered pixels were systematically sampled from the ETM, slope and aspect images, and values were inserted into Equations 2 and 3 to estimate a generalized Minnaert Constant. Pixel BVs were normalized using Equation 4.

Land-Cover Descriptions and Definitions

Land-cover types used were Hardwoods, Mixedwoods, Softwoods, High Mortality, Kampfzone, Krummholz, and Open Rock (Table 1). The WMNF valleys are characterized by Northern Hardwoods forest, with upper slopes and

TABLE 1. SUMMARY TABLE OF LAND-COVER CLASS DEFINITIONS AND DESCRIPTIONS

Definition	Description	Class
Canopy Cover > 10%	FOREST	
Live:Dead Basal Area Ratio > 2.0	Live	
% Live Softwood Canopy > 67%	Live Softwoods	*Softwoods*
% Live Hardwood Canopy > 67%	Live Hardwoods	*Hardwoods*
% Live Hardwood Canopy ≥ 33% AND	Live Mixedwoods	*Mixedwoods*
% Live Softwood Canopy ≤ 67%		
Live:Dead Basal Area Ratio ≤ 2.0	Dead	*High Mortality*
Canopy Cover ≤ 10%	NON-FOREST	
Tree and Sapling Density > 0 stems/m^2	Woody stems present; no canopy	Kampfzone
Tree and Sapling Density = 0 stems/m^2	Alpine	
Twisted/stunted softwoods present	Alpine krummholz vegetation	Krummholz
Twisted/stunted softwoods absent	Tundra, slides, and outcrops	Open Rock

ridges of the red spruce (*Picea rubens*)-balsam fir (*Abies balsamea*) community (Bormann *et al.*, 1970; Reiners and Lang, 1979). Naturally occurring waves of dead balsam fir (fir waves) interrupt the continuity of the softwoods, and represent a major feature of the landscape (Sprugel, 1974; Figure 1). With increasing elevation, Softwoods transition into Kampfzone (Hugentobler, 1994), characterized by nearly pure balsam fir with stems of reduced stature, less than 7.6 cm DBH, and high stem density. Kampfzone vegetation grades into Krummholz, an island patchwork of stunted and twisted balsam fir stems bounded by tracts of boulders and exposed granitic bedrock.

Training Sites and Image Classification

Training sites for the Hardwoods, Mixedwoods, and Softwoods classes were acquired from vegetation plot sampling. In the summer of 1998, 192 stations were located on 34 transects along established hiking trails. Within stations (represented by a 50-m radius circle), four stratified random, 5-m radius plots were placed. Within plots, trees (DBH $\geq$ 7.6 cm) were tallied by DBH size class. Estimates from the four plots were averaged to produce a station estimate. Canopy cover estimates were derived from foliage presence/absence counts using sighting tube densiometers (The GLOBE Program, 1997). The canopy was sampled from 20 locations at 4-meter intervals along two randomly placed transects extending outward from the station center. The best three to five stations representing class definitions were selected as training sites for the Hardwoods, Mixedwoods, and Softwoods classes (Table 1). A 3- by 3-pixel window centered on a selected station defined the training site. It was assumed that a station center coincided with its pixel center, and that training spectra matched sample plot areas. Training sites for the High Mortality, Kampfzone, Krummholz, and Open Rock classes were selected based on photointerpretation of color-infrared (CIR) aerial photography (1:15,840 scale; August 1995) examined with a 3× stereoscope. Training sites were balanced across the "sunshade" (18) and "sunlit" subsets (17). Respective subsets were digitized and stored so that the same sites were applied to all treatments. For treatments not aspect partitioned, the sets were combined, producing a total of 35 training sites.

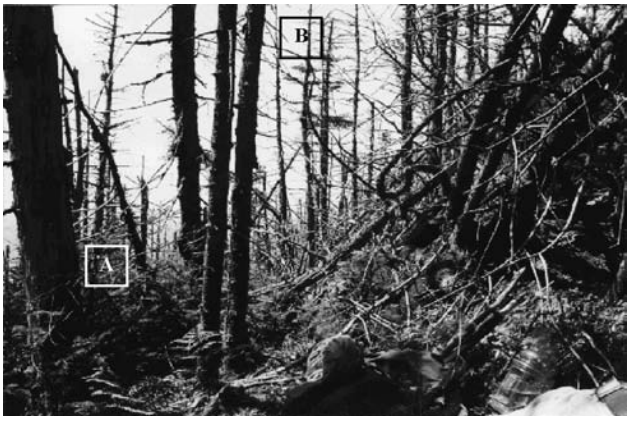

Figure 1. Photograph of fir-wave near summit of Mt. Cabot (Kilkenny, New Hampshire). Note the regenerating balsam fir (*Abies balsamea*) (A), and prevalence of standing dead wood (B).

Four image treatments and a control were classified in feature space using the minimum-distance decision rule for ambiguous pixels (non-invertible signatures precluded use of the maximum-likelihood rule). Treatments I1 and I2 used uncorrected ETM features 4, 5, 7, 5/4 ratio, NDVI, and 4/3 ratio, while treatments I3 and I4 used the same features, except that the BVs were Minnaert Corrected. Treatments I2 and I4 were further Aspect Partitioned into a "sunshade" subset with pixel aspects from 238° (through north) to 56°, and a "sunlit" subset with pixel aspects from 57° to 237° (solar azimuth = 147°; Figure 2). Despite Minnaert Constants generalized from vegetated pixels, the constants were applied without adjustment for the Open Rock class. This class demonstrated signature departures that minimized class confusion, while avoiding additional computational steps. A control classification without any treatment was classified with the full set of training sites using bands 3, 4, 5, and 7. Band 3 was included in the control because treatments had Band 3 information in the NDVI and 4/3 ratio band derivatives.

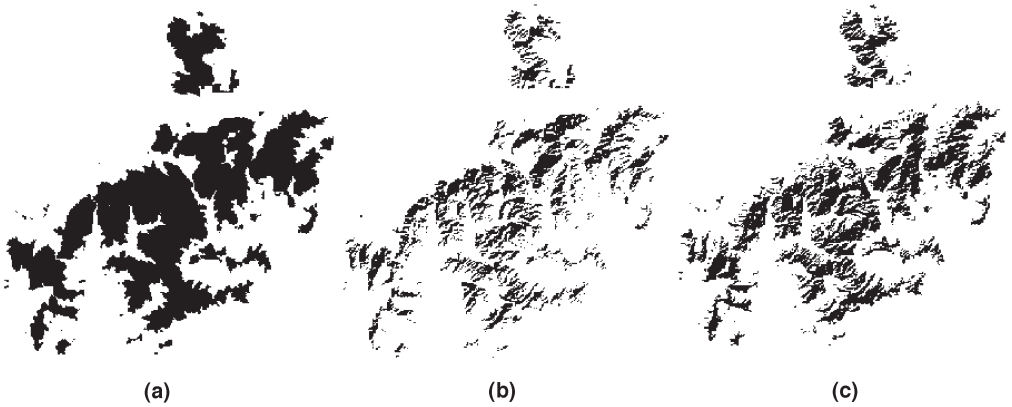

Figure 2. Aspect partitioning of complete data set (a) into two image subsets: (b) "sunshade" pixel aspects ranging from 238° through North to 56°, and (c) "sunlit" pixel aspects ranging from 57° to 237°. The term "sunshade" means pixel orientation is away from the incident solar beam, not in shadow. The solar azimuth was 147°.

Accuracy Assessment

Reference data were collected using CIR aerial photography (see above). Fifty reference polygons per class (Congalton and Green, 1999) were selected, traced onto acetate overlays, digitized onto the imagery, and stored for retrieval and use for all classifications. A polygon was considered labeled correctly if the majority (or a majority tie) of classified pixels' labels agreed with the reference polygon's label.

The Kappa statistic (khat; Congalton, 1991) was used to test the null hypothesis of no difference in treatment Overall Accuracies ($\alpha = 0.05$). The frequency of producing the highest class-specific accuracy (HCSA) from Producer's and User's Accuracies formed a metric for evaluating treatment's class-specific accuracy. This metric ignores the magnitude of accuracy differences, except that treatments share HCSA status if within 5 percentage points of the maximum.

Results

Empirical regression using Equation 3 found the slope of the ordinary least-squares fitted line, which equals the Minnaert Constant ($k_{(\lambda)}$; $\lambda = 3, 4, 5, 7$). The Minnaert Constants and correlation coefficients [$k_{(\lambda)}$ (r)] were 0.29 (0.63), 0.66 (0.58), 0.63 (0.55), and 0.46 (0.57), respectively. Band 3 showed the greatest deviation from the Lambertian assumption ($k_{(\lambda)} = 1$), and Band 4 showed the least deviation. Each $k_{(\lambda)}$ was inserted into the topographical normalization model (Equation 4) and BVs were adjusted for treatments I3 and I4.

Overall accuracy for the control image (49 percent) was much lower than the treatments, which were similar and ranged from 59 percent to 63 percent (Figure 3). The Kappa statistics indicated that the control and all image treatments performed better than random ($P < 0.0001$). However, overall accuracy of the control classification was significantly less than all treatment classifications, and all pair-wise comparisons among treatments showed no significant differences (Table 2). Thus, all treatments outperformed the control, but no treatment performed better than any another.

Variability in class-specific accuracies among treatments was considerably greater than that observed for Overall Accuracy (Table 3). Treatments without aspect partitioning (I1, I3) had the lowest frequency of HCSA for Producer's, User's, and combined accuracies, while treatments with aspect partitioning (I2, I4) had the highest frequency of HCSA (Table 4). Considering class-specific measures of accuracy, image treatment I4 performed best, with I2 next in rank. The control classification had far lower HCSA (2) than even the poorest performing normalization treatment, I1 (5), demonstrating improvement from even modest forms of topographic correction.

Discussion

Determination of the best normalization method(s) was evaluated with an assessment of accuracy of resulting treatment classifications. Differences in treatment overall accuracy were small (59 to 63 percent), and no significant differences in accuracy resulted for any pair-wise comparison among treatments. Therefore, given the choice of approaches tested here, greatest overall accuracy can be achieved with the easiest or most cost-effective normalization treatment. All treatments significantly outperformed the control classification.

Examination of Producer's and User's Accuracies allowed class-specific evaluation of classification performance (Table 4; Story and Congalton, 1986; Congalton, 1991). Among treatments, those without aspect partitioning (I1 and I3) had the lowest HCSA scores. The treatment employing uncorrected band ratios had fewest HCSA occurrences (I1, 5/14), followed by the treatment using both the Minnaert Correction and band ratios (I3, 6/14). Treatments

TABLE 2. PAIRWISE CONTROL AND TREATMENT COMPARISONS OF KHAT TESTING NULL HYPOTHESES (LEFT) CONTROL = I_j AND (RIGHT) $I_j = I_k$ ($\alpha = 0.05$)

Control = I_j	Z score	p	$I_j = I_k$	Z score	p
I1	2.84	0.0023	I1 and I2	−0.63	0.26
I2	3.47	0.0003	I1 and I3	0.00	0.50
I3	2.85	0.0023	I1 and I4	1.18	0.12
I4	4.04	<0.0001	I2 and I3	−0.63	0.26
			I2 and I4	0.55	0.29
			I3 and I4	1.18	0.12

TABLE 3. TREATMENT (CONTROL IN PARENTHESES) RANGES OF PRODUCER'S AND USER'S ACCURACY FOR EACH LAND-COVER CLASS. HW–HARDWOODS, MW–MIXEDWOODS, SW–SOFTWOODS, KZ–KAMPFZONE, KH–KRUMMHOLZ, HM–HIGH MORTALITY, OR–OPEN ROCK

Class	Producer's Accuracy (%)	User's Accuracy (%)
HW	(76) 76–92	(52) 57–68
MW	(28) 34–48	(33) 42–56
SW	(68) 74–90	(35) 49–58
KZ	(24) 20–22	(43) 37–52
KH	(44) 66–76	(55) 60–70
HM	(32) 48–58	(48) 47–53
OR	(68) 72–82	(89) 95–98

TABLE 4. TABLE OF IMAGE TREATMENT CLASSIFICATIONS YIELDING THE HIGHEST CLASS-SPECIFIC ACCURACY (HCSA). LEFT: TREATMENT YIELDING THE HCSA (TIES FOR HCSA OCCURRED IF VALUE WAS WITHIN 5 PERCENTAGE POINTS OF THE MAXIMUM). RIGHT: FREQUENCY OF TREATMENT ATTAINING HCSA. FOR EXAMPLE, I1 HAS TWO OCCURRENCES IN THE PRODUCER'S ACCURACY COLUMN (KZ AND KH), WHERE IT WAS, OR SHARED, THE HIGHEST ACCURACY RANK. HW–HARDWOODS, MW–MIXEDWOODS, SW–SOFTWOODS, KZ–KAMPFZONE, KH–KRUMMHOLZ, HM–HIGH MORTALITY, OR–OPEN ROCK

Treatments with Highest Class Specific Accuracy			Frequency each Treatment Produced the Highest Class Specific Accuracy			
Class	Producer's Accuracy	User's Accuracy	Image Treatment	Producer's Accuracy	User's Accuracy	Combined Accuracy
HW	I3	I2, I4	Control	1	1	2
MW	I2, I4	I2, I4	I1	2	3	5
SW	I4	I1, I3, I4	I2	4	4	8
KZ	C, I1, I2, I3, I4	I3	I3	3	3	6
KH	I1, I3	I1, I4	I4	5	5	10
HM	I2, I4	C, I2				
OR	I2, I4	I1, I2, I3, I4				

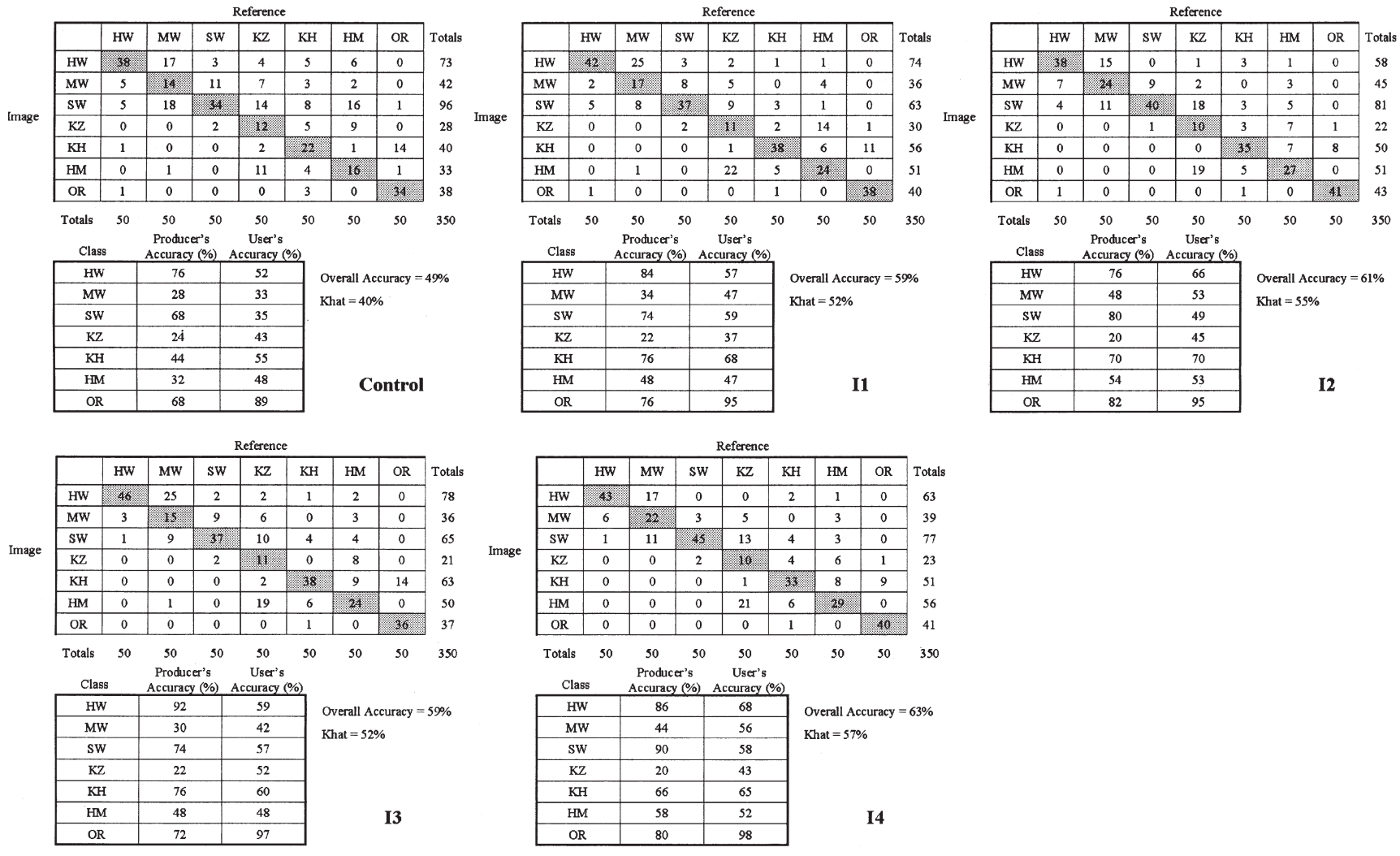

Figure 3. Classification Error Matrices for Control; I1-Without Minnaert Correction or aspect partitioning; I2-Without Minnaert Correction, but with aspect partitioning; I3- With Minnaert Correction, but without aspect partitioning; and I4- With Minnaert Correction and aspect partitioning. HW–Hardwoods, MW–Mixedwoods, SW–Softwoods, KZ–Kampfzone, KH–Krummholz, HM–High Mortality, OR–Open Rock.

using aspect partitioning had a much greater frequency of HCSA (8/14 and 10/14 for I2 and I4, respectively), suggesting that aspect partitioning can contribute more toward increasing class-specific accuracy than can the other methods. The HCSA of treatment I2 was greater than that of I3, which suggests that aspect partitioning and band ratios can provide a greater increase in HCSA than can the Minnaert Correction alone. The treatment with all combinations of techniques (I4) outperformed all others (HCSA = 10/14), suggesting that accuracy increases with contribution from all methods tested here.

All treatments' accuracies outperformed the control classification's overall and HCSA accuracies. Therefore, it is important and efficient to employ even the easiest normalization technique to remove terrain effects. Ranked from easy to hard, band ratios were by far the easiest to employ. The Minnaert Correction was next easiest, because its many computational steps were easily automated. Aspect partitioning was most difficult, because each partition needs to be classified separately, and merged together again.

Few studies have tested the effects of topographic normalization strategies on land-cover classification accuracy. The Minnaert Correction was found to be dependent on wavelength and cover type (Smith *et al.*, 1980; Teillet *et al.*, 1982; Ekstrand, 1996). However, cover-type dependence of $k_{(\lambda)}$ precludes its application in land-cover classification, because spatially explicit cover-type information is sought. In this study, a generalizing assumption grouping forest classes was made for computation of the Minnaert Constant. Using Landsat MSS data, Teillet *et al.* (1982) estimated Minnaert Constants from all cover types (i.e., generalized) and found no overall improvement in classification accuracy imagery versus uncorrected spectral bands for a coastal mountain area in British Columbia. Our results differ, because significant gain in overall accuracy over the uncorrected control resulted from each of the applied treatments. Direct comparison with other studies employing the same treatments was not possible because they did not (1) include controlled multiple image treatments for comparison, or (2) assess the effects on land-cover classification.

Fiorella and Ripple (1993) included incidence angle as a feature to map coniferous seral stages. They compared error matrices for treatments with and without an incidence angle feature, but found no difference in overall accuracy. They did find some class-specific accuracy improvement with the incidence angle feature treatment, but not for classes dominated by coniferous vegetation, and they attributed greater error in labeling coniferous stands to non-Lambertian reflectance. In this study, the conifer dominated classes Softwoods and Krummholz classified well, but Kampfzone and High Mortality performed poorly (20 to 22 percent). Confusion of these classes is understandable because (1) both have open canopies, (2) both are dominated by high stem densities of 1- to 5-m tall balsam fir, and (3) large numbers of standing dead trees within fir-waves appears matched by Kampfzone balsam fir with thick needle-bearing branches on the stems' lower two-thirds, but without needles on the stems' apical one-third. Reflectance from these classes were very similar, and based on structural similarities, they may be united as a class indicative of balsam fir thickets.

Conclusions

Topographic normalization significantly improved classification accuracy over the controlled un-normalized imagery. Overall classification accuracies did not differ among topographic normalization treatments. The highest class-specific accuracies resulted whenever aspect partitioning was used; this suggests that montane classification may be greatly improved by combining the Minnaert Correction with aspect partitioning, or by using aspect partitioning alone. Increases in accuracy with further stratification of aspect are unknown, but should be tested. Aspect partitioning requires independent training sites per image subset and may represent considerable cost if field data collection is used. Use of aerial photography in training site selection from multiple aspect strata may be an economical way to improve land-cover classifications in montane environments.

Calculations for the Minnaert Correction rely on slope and aspect data layers usually derived from a DEM. These DEM derivatives are of questionable accuracy and their effects on the Minnaert Constants are unclear. Band ratios are simplest to calculate and, combined with aspect partitioning, may represent a cost-effective normalization solution.

Acknowledgments

We thank Richard Birnie, Russell Congalton, and Mary Martin for technical assistance and review of the manuscript. We also thank Ryan Huntley, Shannon Spencer, Jay Raymond, Steve Lopez, John Tanzey, and Jim Burnett for field assistance. This research was funded in part by the New Hampshire Space Grant Fellowship Program, NSF Grants (ESI-9452792 and OCE-9903604), and the Garden Club of America's Frances M. Peacock Scholarship for Native Bird Habitat. The manuscript was greatly improved through comments from three anonymous reviewers.

References

Bormann, F.H., T.G. Siccama, G.E. Likens, and R.H. Whittaker, 1970. The Hubbard Brook ecosystem study: Composition and dynamics of the tree stratum, *Ecological Monographs*, 40:373–388.

Brown, D.G., and T.J. Bara, 1994. Recognition and reduction of systematic error in elevation and derivative surfaces from 7.5-minute DEMs, *Photogrammetric Engineering & Remote Sensing*, 60(2):189–194.

Civco, D.L., 1989. Topographic normalization of Landsat Thematic Mapper digital imagery, *Photogrammetric Engineering & Remote Sensing*, 55(9):1303–1309.

Colby, J.D., 1991. Topographic normalization in rugged terrain, *Photogrammetric Engineering & Remote Sensing*, 57(5):531–537.

Congalton, R.G., 1991. A review of assessing the accuracy of classifications of remotely sensed data, *Remote Sensing of Environment*, 37:35–46.

Congalton, R.G., and K. Green., 1999. *Assessing the Accuracy of Remotely Sensed Data: Principles and Practices*, CRC Press, Boca Raton, Florida, 137 p.

Ekstrand, S., 1994. Assessment of forest damage with Landsat TM: Correction for varying forest compartment characteristic's assessment of damage, *Remote Sensing of Environment*, 47:291–302.

———, 1996. Landsat TM-based forest damage assessment: Correction for topographic effects, *Photogrammetric Engineering & Remote Sensing*, 62(2):151–161.

Fiorella, M., and W.J. Ripple, 1993. Determining successional stage of temperate coniferous forests with Landsat satellite data, *Photogrammetric Engineering & Remote Sensing*, 59(2):239–246.

Globe Program, 1997. *The GLOBE Teacher's Guide*, GLOBE Program, Washington, D.C., 256 p.

Holben, B.N., and C.O. Justice, 1980. The topographic effect on spectral response from nadir-pointing sensors, *Photogrammetric Engineering & Remote Sensing*, 46(9):1191–1200.

Hugentobler, O., 1994. Waldgrenze und Kampfzone, *Bündnerwald*, 47(1):43–52.

Minnaert, M., 1941. The reciprocity principle in lunar photometry, *Astrophysical Journal*, 93:403–410.

Noon, B.R., 1981. Techniques for sampling avian habitats, *The Use of Multivariate Statistics in Studies of Wildlife Habitat* (D. E. Capen, editor), United States Forest Service General Technical Report RM-87, Fort Collins, Colorado, pp. 42–50.

Reiners, W.A., and G.E. Lang, 1979. Vegetational patterns and processes in the balsam fir zone, White Mountains, New Hampshire, *Ecology*, 60(2):403–417.

Rock, B.N., J.E. Vogelmann, D.L. Williams, A.F. Vogelmann, and T. Hoshizaki, 1986. Remote detection of forest damage, *Bioscience*, 36(7):439–445.

Smith, J.A., T.L. Lin, and K.J. Ranson, 1980. The Lambertian assumption and Landsat data, *Photogrammetric Engineering & Remote Sensing*, 46(9):1183–1189.

Sprugel, D.G., 1974. Dynamic structure of wave-regenerated Abies balsamea forests in the North-eastern United States, *Journal of Ecology*, 64:889–911.

Story, M., and R. Congalton, 1986. Accuracy assessment: a user's perspective, *Photogrammetric Engineering & Remote Sensing*, 52(3):397–399.

Teillet, P.M., B. Guindon, and D.G. Goodenough, 1982. On the slope-aspect correction of Multispectral Scanner data, *Canadian Journal of Remote Sensing*, 8(2):84–106.

Vogelmann, J.E., 1990. Comparison between two vegetation indices for measuring different types of forest damage in the northeastern United States, *International Journal of Remote Sensing*, 11(12):2281–2297.

Vogelmann, J.E., and B.N. Rock, 1988. Assessing forest damage in high-elevation coniferous forests in Vermont and New Hampshire using Thematic Mapper data, *Remote Sensing of Environment*, 24:227–246.

———, 1989. Use of Thematic Mapper data for the detection of forest damage caused by pear thrips, *Remote Sensing of Environment*, 30:217–225.

(Received 24 September 2001; revised and accepted 04 October 2002)